Journal of Hazardous Materials 217–218 (2012) 406–415

Contents lists available at SciVerse ScienceDirect

Journal of Hazardous Materials

journal homepage: www.elsevier.com/locate/jhazmat

Synthesis, characterization and adsorption properties of diethylenetriamine-modified hypercrosslinked resins for efficient removal of salicylic acid from aqueous solution

Jianhan Huang[a,*], Xiaoying Jin[a], Jinglin Mao[a], Bin Yuan[b], Rujie Deng[b], Shuguang Deng[b,**]

[a] School of Chemistry and Chemical Engineering, Central South University, Changsha, Hunan 410083, China
[b] Chemical Engineering Department, New Mexico State University, Las Cruces, NM 88003, USA

ARTICLE INFO

Article history:
Received 11 January 2012
Received in revised form 14 March 2012
Accepted 17 March 2012
Available online 26 March 2012

Keywords:
Adsorption
Equilibrium
Kinetics
Breakthrough
Salicylic acid
Hypercrosslinked resins

ABSTRACT

We report an effective approach for tailoring the pore textural properties and surface polarity of a hypercrosslinked resin to enhance its adsorption capacity and selectivity for removing salicylic acid from aqueous solution. Four hypercrosslinked resins were synthesized by controlling the reaction time of the self Friedel–Crafts reaction of chloromethylated polystyrene-co-divinylbenzene, and then modified with diethylenetriamine to adjust their surface polarity. The resins were characterized with N_2 adsorption for pore textural properties, Fourier transform infrared spectroscopy (FT-IR) for surface functional groups, chemical analysis for residual chlorine content and weak basic exchange capacity. Adsorption equilibrium, kinetics and breakthrough performance were determined for the removal of salicylic acid from aqueous solution on a selected resin HJ-M01. The equilibrium adsorption capacity of salicylic acid on HJ-M01 is significantly higher than that on its precursor HJ-11 and a few commercial adsorbents including AB-8, XAD-4 and XAD-7. The dynamic adsorption capacity of salicylic acid on HJ-M01 was found to be 456.4 mg/L at a feed concentration of 1000 mg/L and 294 K. The used resin could be fully regenerated with 1% sodium hydroxide solution. The hypercrosslinked resins being developed were promising alternatives to commercial adsorbents for removing salicylic acid and other volatile organic compounds (VOCs) from aqueous solution.

1. Introduction

Wastewater contaminated by aromatic compounds such as phenol, β-naphthol, salicylic acid and other volatile organic compounds (VOCs) is a significant concern to the biological system and the environment due to the high toxicity and very slow biodegradation of these organic compounds [1,2]. Therefore, remediation of aromatic compounds-containing wastewater is an imminent and important issue for environmental protection. In recent years, a wide range of physical and chemical technologies including photo-catalytic oxidation, membrane separation, electrochemical oxidation, solvent extraction, ion exchange and adsorption are employed for aromatic compounds removal from aqueous solution [3–7]. Among which the adsorption-based process is probably the most favorable treatment option due to its efficacy, practicality and economic feasibility [8,9]. Additionally, adsorption is also widely used for treatment of dye, heavy metals and other organic/inorganic hazardous impurities from aqueous solution [10].

Due to its unique structure and extraordinary adsorption properties, the hypercrosslinked polystyrene-co-divinylbenzene (PS) resin is proven to be an efficient polymeric adsorbent for adsorptive removal of aromatic compounds such as benzene, toluene, β-naphthol and phenol from aqueous solution [11,12]. This resin has a high adsorption capacity for aromatic compounds, it can be reused for more than 50 cycles and is being considered as a potential replacement of activated carbon for organic compounds removal from wastewater [13]. In addition, this type of resin has also been used as column packing materials in high-performance liquid chromatography (HPLC), ion size-exclusion chromatography materials and solid-phase extraction materials for gases, organic contaminants and organic vapors [14–16]. In general, this type of resin is synthesized from a linear PS or a low cross-linked PS by adding bi-functional cross-linking reagents such as monochloromethylether, *p*-dibenzenylchloride and *p*-dichloromethylbenzene, and Friedel–Crafts catalysts including anhydrous zinc chloride, iron (III) chloride and stannic (IV) chloride. They can also be prepared from a macroporous low cross-linked chloromethylated PS via its self Friedel–Crafts reaction [17].

* Corresponding author. Tel.: +86 731 88879850; fax: +86 731 88879616.
** Corresponding author. Tel.: +1 575 646 4346; fax: +1 575 646 7706.
E-mail addresses: jianhanhuang@csu.edu.cn (J. Huang), sdeng@nmsu.edu (S. Deng).

0304-3894/$ – see front matter © 2012 Elsevier B.V. All rights reserved.
doi:10.1016/j.jhazmat.2012.03.053

After the corresponding reactions, the obtained hypercrosslinked PS networks consist of an intensive bridging of strongly solvated PS chains with conformationally rigid links, leading to a major shift of their pore diameter distribution from predominately mesopores to mesopores–micropores bimodal distribution, and hence results in a sharp increase of the Brunauer–Emmet–Teller (BET) surface area and pore volume [18,19]. Because of these significant changes, the hypercrosslinked resin displays very large adsorption capacities towards non-polar and weakly polar aromatic compounds in aqueous solution. In order to increase their adsorption capacities towards polar aromatic compounds, the resins are often modified by introducing polar units into the copolymers, using polar compounds as the cross-linking reagent and addition of polar compounds in the Friedel–Crafts reaction [20,21]. The results indicate that the chemically modified hypercrosslinked resins exhibit improved adsorption properties towards polar aromatic compounds by introducing certain specific functional groups on the surface [22].

For the self Friedel–Crafts reaction of macroporous low crosslinked chloromethylated PS, it was found out that the residual chlorine content in the synthesized hypercrosslinked resin declined sharply at the beginning of reaction, and then slowly and gradually decreased when the reaction preceded further [23]. We hypothesize that the pore textural properties and the surface functionality of the hypercrosslinked resins critically depends on the residual chlorine content in the final product. Therefore, we believe that it is feasible to tailor the pore structure and surface functionality by simply controlling the residual chlorine content in the hypercrosslinked resins. We can manipulate the pore textural properties of the resins by controlling of the self Friedel–Crafts reaction time, and then adjust the resins' surface functionality by uploading specific functional groups. This allows us to synthesize polymeric adsorbents with adjustable adsorption selectivity towards aromatic compounds of different polarities. To the best of our knowledge, this reaction time control approach for optimizing the hypercrosslinked resins for wastewater treatment is not reported in the literature yet.

In this study, we firstly synthesized four hypercrosslinked resins from macroporous low crosslinked chloromethylated PS through the self Friedel–Crafts reaction with different Friedel–Crafts reaction times. These hypercrosslinked resins were then chemically modified by the amination reaction via diethylenetriamine to produce the diethylenetriamine-modified hypercrosslinked resins. Thereafter, the high adsorption selectivity towards aromatic compounds, β-naphthol, phenol and salicylic acid on these four resins was confirmed by the batch adsorption experiments. The most promising sample labeled as HJ-M01 was selected for detailed experimental studies for the adsorptive removal of salicylic acid from aqueous solution. The adsorption equilibrium, kinetics and breakthrough dynamics of salicylic acid on the adsorbent HJ-M01 were measured and analyzed in detail.

2. Experimental

2.1. Synthesis and characterization of diethylenetriamine-modified hypercrosslinked resins

As an established synthesis procedure [11–14,17], the hypercrosslinked resin is usually synthesized from chloromethylated PS using nitrobenzene as the solvent and anhydrous zinc chloride as the catalyst. Because nitrobenzene is a highly toxic reagent, in this study, we used 1,2-dichloroethane to replace it as the solvent and anhydrous iron (III) chloride as the catalyst. As shown in Scheme 1, 25 g of chloromethylated PS (Langfang Chemical Co. Ltd., China; chlorine content: 17.3%; particle size: 20–40 mesh) was swollen in 120 ml of 1, 2-dichloroethane (A.R., Sigma–Aldrich; residual water was removed by molecular sieve before using) overnight. At a moderate mechanical stirring speed, the temperature of the reaction mixture was increased to 323 K and 5 g of anhydrous iron (III) chloride (A.R., Sigma–Aldrich; used without further purification) was added into the reaction mixture. After half an hour, the reaction mixture was refluxed for 1 h, 3 h, 5 h and 9 h, respectively, and the obtained hypercrosslinked resins were named as HJ-11, HJ-33, HJ-55 and HJ-99 accordingly. After rinsing, 20 g of the precursor resin was mixed with 60 ml of diethylenetriamine (A.R., Sigma–Aldrich) and the reaction mixture was kept at 413 K for 20 h with N_2 protection, and the corresponding diethylenetriamine-modified hypercrosslinked resins labeled as HJ-M01, HJ-M03, HJ-M05 and HJ-M09 were prepared.

The chorine content in the resins was measured by the Volhard method [24] and the weak basic exchange capacity of the resin was determined by another established method [25]. The BET specific surface area, *t*-plot micropore surface area, pore volume, *t*-plot micropore volume and pore diameter distribution of the samples were determined from the N_2 adsorption–desorption isotherms 77 K using a Micromeritics Tristar 3000 surface area and porosity analyzer. The Fourier transform infrared spectroscopy (FT-IR) of the resins was collected by KBr disks on a Nicolet 510P Fourier transformed infrared instrument.

2.2. Adsorption experiments

For adsorption equilibrium measurements, about 0.1000 g of the sample was mixed with 50 ml solution containing 200–1000 mg/L of β-naphthol ($C_{10}H_7OH$, molecular weight: 144.2; A.R., Sigma–Aldrich), or phenol (C_6H_5OH, molecular weight: 94.1; A.R., Sigma–Aldrich), or salicylic acid (C_6H_4(*o*-OH)COOH, molecular weight: 138.1; A.R., Sigma–Aldrich) in a 100 ml conical flask. The series of flasks were then shaken in a thermostatic oscillator at a desired temperature (294, 304 or 314 K) and an agitation speed of 180 rpm until adsorption equilibrium was reached after about eight hours. To determine the equilibrium concentration of salicylic acid in the solution, a working curve of UV absorbency-concentration was firstly developed. The absorbency of a standard salicylic acid solution with different known concentrations was analyzed by a UV-2450 spectrophotometer at the wavelength of 296.5 nm. A well-fitted regression equation, $A = 0.02384C + 0.0369$, was obtained with a correlation coefficient R^2 of 0.9999. Then the absorbency of the salicylic acid solution adsorbed by the resin was measured and the equilibrium concentration of salicylic acid C_e (mg/L) was calculated based on the working curve. The equilibrium adsorption capacity q_e (mg/g) was determined based on the following material balance equation:

$$q_e = \frac{(C_0 - C_e)V}{W} \quad (1)$$

where C_0 is the initial concentration (mg/L), V the volume of the solution (L) and W the mass of the resin (g). The corresponding adsorption isotherm at a given temperature was obtained by plotting the equilibrium adsorption capacity with the equilibrium concentration.

For the adsorption kinetic experiments, about 1.0000 g of resin was mixed with 250 ml of a salicylic acid solution in a 250 ml conical flask, and the initial concentrations of salicylic acid of 300, 500 and 1000 mg/L were used in these experiments. The flask was then continuously shaken at a desired temperature (294 or 304 K) until adsorption equilibrium was reached. In this process, 0.5 ml of the solution was withdrawn at a ten-minute interval in the first hour and a sixty-minute interval in the subsequent hour and the

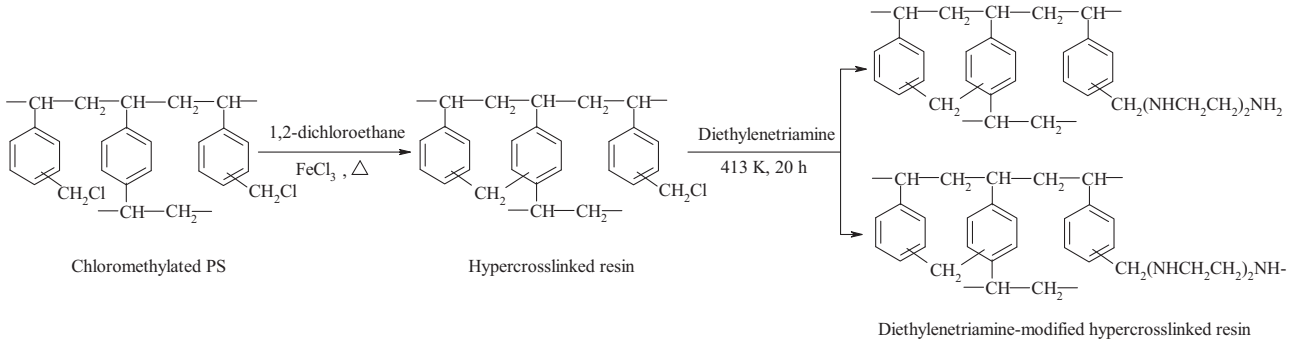

Scheme 1. Synthetic procedure of the hypercrosslinked resin and diethylenetriamine-modified hypercrosslinked resin.

concentration of salicylic acid was determined, the adsorption capacity at a contact time t was calculated as:

$$q_t = \frac{(C_0 - C_t)V}{W} \quad (2)$$

where q_t is the adsorption capacity at a contact time t (mg/g) and C_t is the concentration at contact time t (mg/L). The adsorption kinetic curve was obtained by plotting the adsorption capacity with contact time t.

For the dynamic adsorption-desorption experiments, about 3.0 g of resin were firstly immersed in de-ionized water at 294 K for 24 h, and then packed in a glass column densely without bubbles in the column. The salicylic acid solution with an initial concentration of 1000.0 mg/L was passed through the resin column at a flow rate of 6.0 BV/h (1 BV = 10 ml) and the concentration of salicylic acid in the effluent from the column exit, C_v (mg/L), was continuously recorded until it reached the feed concentration. After the adsorption breakthrough run, the resin column was repeatedly rinsed with de-ionized water until the effluent from the column was free of salicylic acid. Then a 1% sodium hydroxide aqueous solution were applied to the desorption process. 300 ml of sodium hydroxide aqueous solution were passed through the resin column at a flow rate of 5.4 BV/h and the concentration of salicylic acid was determined. A second adsorption breakthrough experimental run was repeated after the resin column was regenerated. The dynamic adsorption curve was plotted by using C_v/C_0 as the ordinate and volume of the effluent as the abscissa whereas the desorption dynamic curve was plotted by using the effluent concentration of salicylic acid as the ordinate and the desorption bed volume as the abscissa.

3. Results and discussion

3.1. Characteristics of the samples

As can be seen from Table 1, the residual chlorine content in the synthesized hypercrosslinked resins, HJ-11, HJ-33, HJ-55 and HJ-99, sharply decreased from 17.3% in the chloromethylated PS after the Friedel–Crafts reaction, implying that the chlorine of the chloromethylated PS was consumed in the self Friedel–Crafts reaction. Additionally, the residual chlorine content was further reduced with increasing of the reaction time. In particular, the residual chlorine content decreased faster at the beginning of the reaction and then gradually decreased as the reaction proceeded, these observations were consistent with the reported results [23].

After the reaction between the hypercrosslinked resin and diethylenetriamine, the residual chlorine content in the obtained resins was further reduced and the final chlorine content in all of the diethylenetriamine-modified hypercrosslinked resins was roughly equivalent, indicating that the chlorine in the chloromethylated PS was further substituted. The amounts of the uploaded amino groups on the surface of the resins should be different with HJ-M01 having the highest uploading amount while HJ-M09 having the least among the four resins.

The differences of residual chlorine content between the hypercrosslinked resins, HJ-11, HJ-33, HJ-55 and HJ-99, and the diethylenetriamine-modified hypercrosslinked resins, HJ-M01, HJ-M03, HJ-M05 and HJ-M09, can be calculated to be 1.307, 0.792, 0.744 and 0.594 mmol/g, respectively. These data are quite different from the weak basic exchange capacities determined by the chemical analysis (see Table 1). This is because one diethylenetriamine molecule having three amino groups (two —NH_2 and one —NH—) can react with one, two or three chlorine atoms in the hypercrosslinked resin, and the weak basic exchange capacity of the diethylenetriamine-modified hypercrosslinked resin will be tripled, sesquialtered, or no change accordingly. The values of the weak basic exchange capacities suggest that one or two chlorine atoms in the hypercrosslinked resin are substituted in the amination reaction with diethylenetriamine. The sample HJ-M01 is the most polar resin while HJ-M09 is the least polar resin among the four samples.

Fig. 1(A) shows the N_2 adsorption–desorption isotherms of the obtained hypercrosslinked resins and the diethylenetriamine modified hypercrosslinked resins and he pore textural properties for all the samples are summarized in Table 1. The N_2 adsorption amount on the hypercrosslinked resins increases with increasing of the self Friedel–Crafts reaction time, suggesting that a longer reaction time results in higher BET surface area and pore volume. The N_2 adsorption amounts, BET surface area of the diethylenetriamine-modified resins (HJ-M01, HJ-M03, HJ-M05 and HJ-M09) are smaller than the corresponding un-modified resins (HJ-11, HJ-33, HJ-55 and HJ-99), which is probably due to the uploading of amino groups on the hypercrosslinked resin has partially blocked the micropores and therefore reduces the micropore volume and the BET surface area. It is also expected that a higher uploading amount of amino groups leads a larger decrease in the BET surface area and pore volume. However, uploading amino groups on the hypercrosslinked resin can increase the polarity of the resins. The N_2 adsorption isotherms on all of the resins are of type-II. The sharp increase of N_2 adsorption amount at the initial pressure range ($p/p_0 < 0.05$) is an evidence of adsorption in micropores. The visible hysteresis loop of the N_2 desorption isotherms suggests that these resins also have some mesopores. As shown in Fig. 1(B), these samples have a wide pore diameter distribution ranging from less than 2 nm to 180 nm (micropore to macropore). We have demonstrated the feasibility of tailoring the pore textural properties and surface functionality of hypercrosslinked resins by adjusting their residual chorine content using the Friedel–Craft time as an important controlling parameter.

The FT-IR spectra of all the samples are displayed in Fig. 2(A). After the Friedel–Crafts reaction, all of the vibrational peaks remained the same except for the representative strongest peak

Table 1
The characteristic parameters for the hypercrosslinked resins, HJ-11, HJ-33, HJ-55, HJ-99, and diethylenetriamine-modified hypercrosslinked resins, HJ-M01, HJ-M03, HJ-M05, HJ-M09.

	Residual chlorine content (%)	Weak basic exchange capacity (mmol/g)	Water retention capacity (%)	BET surface area (m^2/g)	*t*-Plot micropore surface area (m^2/g)	Pore volume (cm^3/g)	*t*-Plot micropore volume (cm^3/g)
HJ-11	5.42	–	–	834.5	451.6	0.5504	0.2436
HJ-33	3.50	–	–	910.8	497.8	0.5938	0.2684
HJ-55	3.15	–	–	941.7	514.2	0.6137	0.2768
HJ-99	2.45	–	–	1040.1	600.7	0.6554	0.3239
HJ-M01	0.78	3.202	64.2%	626.9	375.7	0.4052	0.2051
HJ-M03	0.69	2.010	60.8%	658.2	394.6	0.4258	0.2151
HJ-M05	0.51	1.804	57.4%	746.4	475.7	0.4487	0.2574
HJ-M09	0.44	0.902	56.1%	972.8	551.1	0.6240	0.2971

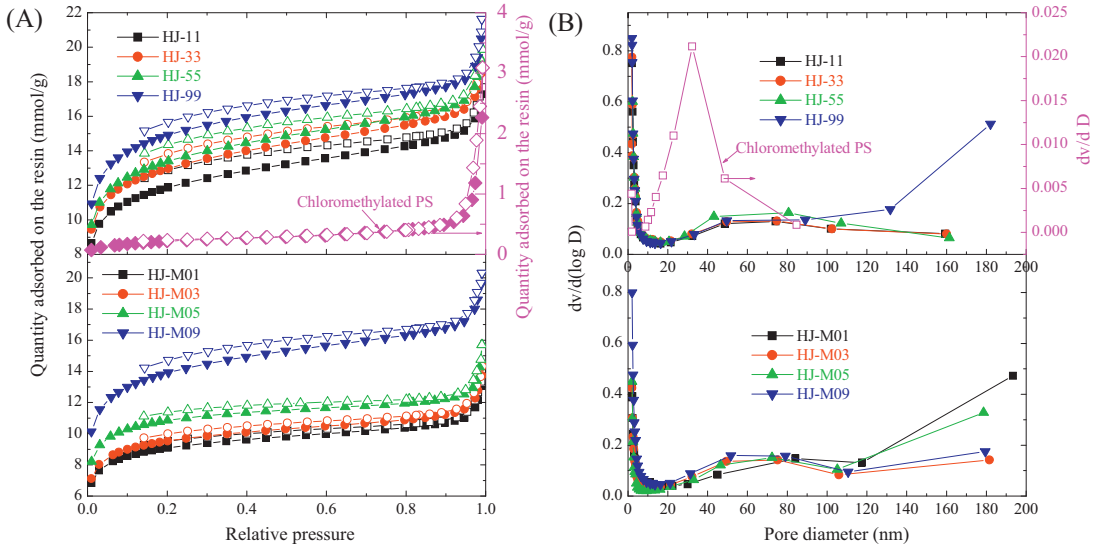

Fig. 1. N_2 adsorption–desorption isotherms of the hypercrosslinked resins, HJ-11, HJ-33, HJ-55 and HJ-99 as well as those of the diethylenetriamine-modified hypercrosslinked resins, HJ-M01, HJ-M03, HJ-M05 and HJ-M09 (A); and corresponding pore diameter distributions (B).

of CH_2Cl groups at 1265 cm^{-1}, which was significantly weakened [26]. In addition, a moderate C=O stretching vibration appears at 1705 cm^{-1} for the four hypercrosslinked resins. In the Friedel–Crafts reaction system using nitrobenzene as the solvent, this peak is assigned to the formaldehyde carbonyl groups, and appearance of this peak is resulted from oxidation of CH_2Cl groups and nitrobenzene as well as the oxygen in the air is considered as the oxidizer [27,28]. Therefore, oxidation of CH_2Cl groups is also observed in this work. After the reaction between the hypercrosslinked resin and diethylenetriamine, a strong vibrational band with a frequency at 3426 cm^{-1} is seen, which can be associated with the N—H stretching of —NH— or $—NH_2$ groups [26]. In addition, the vibrational band at 1501 cm^{-1} related to the N—H deformation of —NH— or $—NH_2$ groups and that at 1109 cm^{-1} concerned

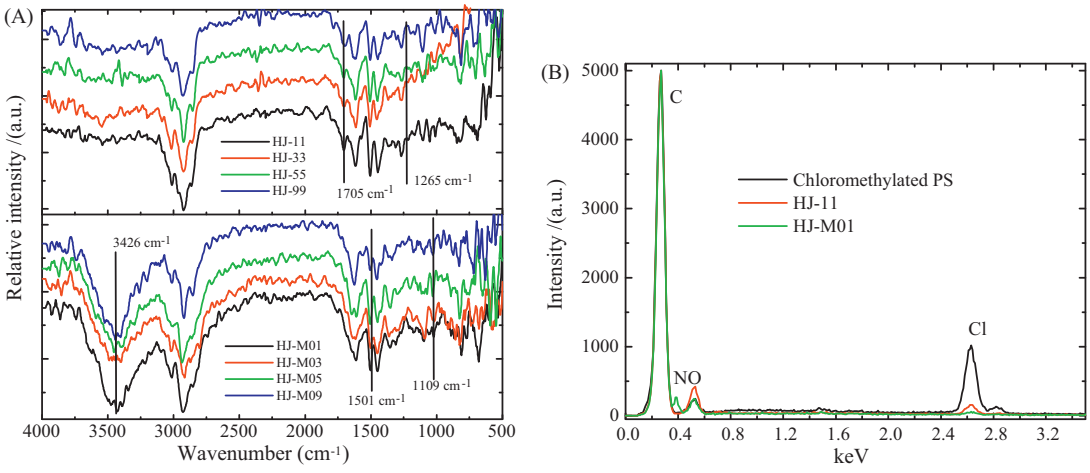

Fig. 2. (A) FT-IR spectra of the hypercrosslinked resins, HJ-11, HJ-33, HJ-55 and HJ-99 as well as those of the diethylenetriamine-modified hypercrosslinked resins, HJ-M01, HJ-M03, HJ-M05 and HJ-M09; and (B) the energy dispersive X-ray spectroscopy (EDS) spectra of the chloromethylated PS, HJ-11 and HJ-M01.

with the C—N stretching also confirmed the successful uploading of diethylenetriamine on the surface of the hypercrosslinked resin.

Fig. 2(B) depicts the energy dispersive X-ray spectroscopy (EDS) spectra for the chloromethylated PS, HJ-11 and HJ-M01 samples. The chlorine content of HJ-11 was much lower than that of chloromethylated PS, which is consistent with the FT-IR results that the chlorine content was sharply decreased after the Friedel–Crafts reaction. On the other hand, the oxygen content of HJ-11 was obviously increased after the Friedel–Crafts reaction, which agreed with the results of the FT-IR spectrum that there appears a new moderate vibration related to the C=O stretching at 1705 cm^{-1} for the hypercrosslinked resin. In addition, Fig. 2(B) indicated that the chlorine content of HJ-M01 was further reduced in comparison with HJ-11 while there appeared a new small peak related to the nitrogen atom in the EDS spectrum of HJ-M01, which implied that diethylenetriamine was successfully uploaded on the surface of the resin. This deduction is also consistent with the previous results of the FT-IR spectrum showing the N-H stretching, N—H deformation and C—N stretching of the amino groups in the diethylenetriamine-modified hypercrosslinked resin. The scanning electron microscopy (SEM) images of HJ-M01 are shown in Fig. 3. HJ-M01 is a spherical solid particle with a particle size about 0.5 mm and its surface is rough with many fissures.

3.2. Adsorption selectivity

Fig. 4 compares the adsorption capacity of β-naphthol, phenol and salicylic acid on HJ-M01, HJ-M03, HJ-M05 and HJ-M09 at a temperature of 294 K. It is obvious that the adsorption capacity of β-naphthol on HJ-M09 is the largest, and that of phenol on HJ-M05 is the largest while that of salicylic acid on HJ-M01 is the largest among the four resins. The BET surface area as well as pore structure of the resin, the polarity matching between the resin and the adsorbate, and the size matching between the pore diameter of the resin and the molecular size of the adsorbate are thought to be the main factors influencing the adsorption [29,30]. β-naphthol has the least polarity among the three adsorbates [31], hence it is expected that the resin HJ-M09 which possessed the highest BET surface area, pore volume and the least polarity has the largest adsorption capacity towards β-naphthol. HJ-M01 has the least BET surface area and pore volume, while it has the highest uploading amount of amino groups and the greatest polarity among the four resins, hence it is expected that HJ-M01 has the largest adsorption capacity towards the most polar adsorbate (salicylic acid), and the possible hydrogen bonding between the phenolic hydroxyl, carboxyl groups of salicylic acid and amino groups of HJ-M01 will enhance the adsorption [32]. In conclusions, we have successfully demonstrated the feasibility of manipulating the pore textural properties and surface functionality of the hypercrosslinked resins for adsorption of VOCs with different polarity.

3.3. Comparison of adsorption of salicylic acid on different adsorbents

To testify the necessity of chemical modification of the hypercrosslinked resin by uploading the amino groups, the adsorption isotherms of salicylic acid on HJ-11 and HJ-M01 at 294 K are compared in Fig. 5(A). The adsorption capacity of salicylic acid on HJ-M01 is significantly larger than that on HJ-11. Although the BET surface area of HJ-11 is higher than that of HJ-M01 (difference: 207.6 m^2/g), the uploaded amino groups on the surface of HJ-M01 enhanced the adsorption of salicylic acid on HJ-M01 due to the polarity matching and the possible hydrogen bonding between the amino groups of HJ-M01 and the phenolic hydroxyl, carboxyl groups of salicylic acid. Activated carbon is one of the most widely used adsorbents for adsorption of VOCs from

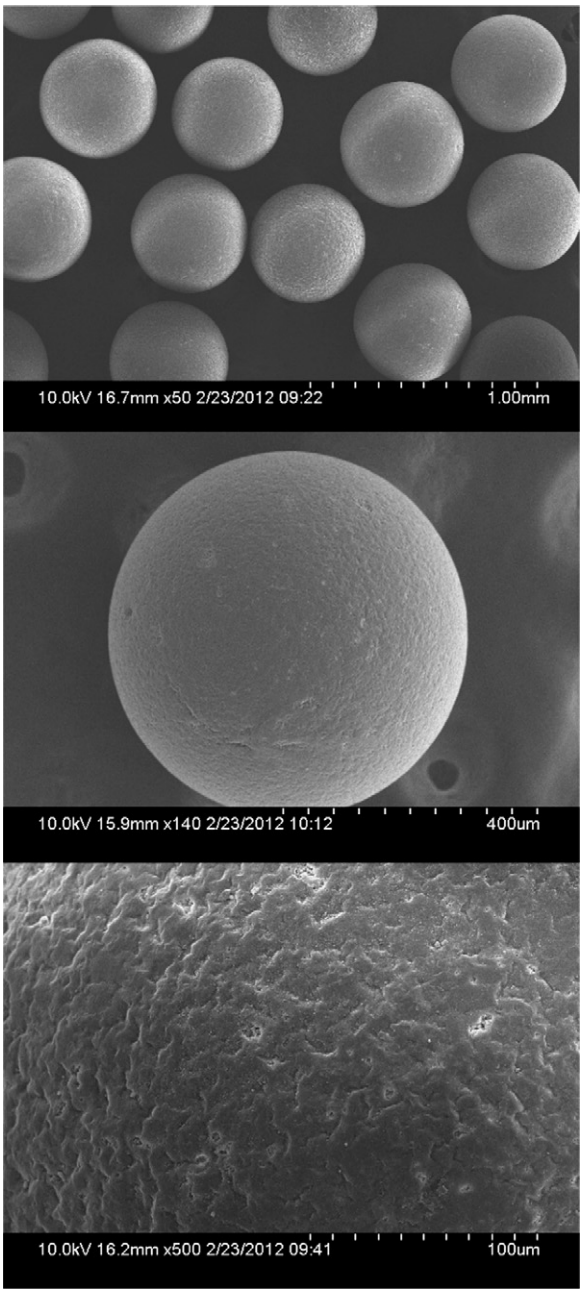

Fig. 3. Scanning electron microscopy (SEM) images of HJ-M01.

wastewater. As compared the adsorption of salicylic acid on HJ-M01 with that on activated carbon [33], HJ-M01 is shown to be almost the same efficient as the activated carbon for adsorption of salicylic acid from aqueous solution. Some low-cost materials or even wastes such as bentonite, kaolinite, hematite and calcite seem economically attractive for practical application of salicylic acid from aqueous solution [34–37]. However, these materials are inferior to HJ-M01 for adsorption of salicylic acid. In addition, as compared the adsorption of salicylic acid on HJ-M01 with some other polymeric adsorbents reported in the literatures [38–41], HJ-M01 is also proven superior to some nonionic polymeric resins and hypercrosslinked resins.

Many commercial adsorbents including AB-8 (bought from the Chemical Plant of Nankai University, China), XAD-4 and XAD-7 (kindly provided by Rohm & Haas Company, Philadelphia, USA) are considered the most efficient polymeric adsorbents for adsorptive removal of aromatic pollutants from wastewater [42–44]. The

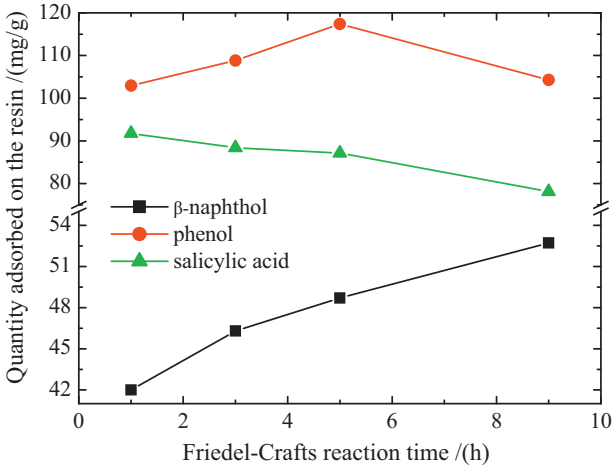

Fig. 4. Comparison of adsorption capacity of β-naphthol, phenol and salicylic acid on HJ-M01, HJ-M03, HJ-M05 and HJ-M09 from aqueous solution containing 104 mg/L of β-naphthol, or 500 mg/L of phenol, or 200 mg/L of salicylic acid at 294 K.

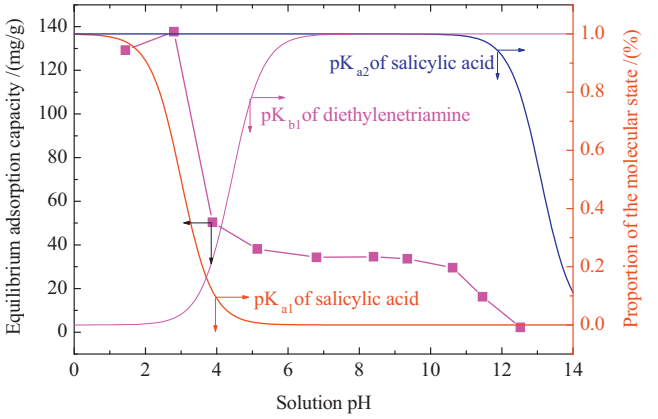

Fig. 6. Solution pH effect on the adsorption of salicylic acid on adsorbent HJ-M01 with the temperature at 294 K.

adsorption isotherm of salicylic acid on HJ-M01 at 294 K is then compared with those on AB-8, XAD-4 and XAD-7 in Fig. 5(B). The adsorption capacity of salicylic acid on HJ-M01 is much larger than that on AB-8, XAD-4 and XAD-7. The BET surface area and pore volume of HJ-M01 are slightly lower than those of AB-8 (880 m^2/g and 1.08 cm^3/g), XAD-4 (725 m^2/g and 0.98 cm^3/g), and somewhat higher than those of XAD-7 (450 m^2/g and 1.14 cm^3/g) and AB-8 (480-520 m^2/g and 0.73-0.77 cm^3/g). These results further confirmed that not only the BET surface area and pore volume of the resin but also the polarity matching between the resin and the adsorbate strongly affect the adsorption capability of the resin. This encouraging result strongly suggests that the new polymeric adsorbent being developed in our laboratory is promising replacement for many commercial adsorbents for aromatic pollutants and other VOCs from wastewater.

Langmuir and Freundlich models are the two typical adsorption isotherm models for describe adsorption of organic compounds from aqueous solution [45,46]. The Langmuir model assumes that the adsorption occurs on a structurally homogeneous adsorbent and all the adsorption sites are energetically identical, the linear Langmuir equation is given by:

$$\frac{C_e}{q_e} = \frac{C_e}{q_m} + \frac{1}{q_m K_L} \quad (3)$$

where q_m is the monolayer adsorption capacity (mg/g), and K_L is a constant related to adsorption energy (L/mg) [47]. The Langmuir equation constants were obtained from the intercepts and slopes of linear correlations of experimental isotherm data with the Langmuir equation.

The Freundlich equation describes the adsorption on a heterogeneous surface and its linear form can be expressed as:

$$\log\ q_e = \frac{1}{n} \log C_e + \log K_F \quad (4)$$

where K_F [(mg/g)(L/mg)$^{1/n}$] and n are the characteristic constants.

The linear Langmuir and Freundlich equations were used to correlate the adsorption isotherms in this work, the corresponding parameters q_m, K_L, K_F and n, as well as the correlation coefficients R^2 are summarized in Tables S1 and S2. The Langmuir model appears to be more suitable for most of the adsorption isotherm data on HJ-M01 ($R^2 > 0.99$), while the Freundlich model is more suitable for describing the adsorption on XAD-4 and XAD-7, and none of them is not suitable for the adsorption on AB-8.

3.4. Effect of solution pH on adsorption

As shown in Fig. 6, the adsorption of salicylic acid on HJ-M01 is very sensitive to the solution pH. According to the reported pK_{a1} (2.98) and pK_{a2} (13.1) of salicylic acid in aqueous solution [48], the dissociation curve of salicylic acid as well as that of the mono-anion of salicylic acid in aqueous solution are predicted as a function of the solution pH. As the solution pH is in the range of 2.80–10.62, the adsorption of salicylic acid on HJ-M01 has the same trend as the dissociation curve of salicylic acid. Meanwhile, the tendency of the adsorption is similar to the dissociation curve of the mono-anion of salicylic acid as the solution pH increases from 10.62 to 12.52. These observations imply that the molecular form of salicylic acid is

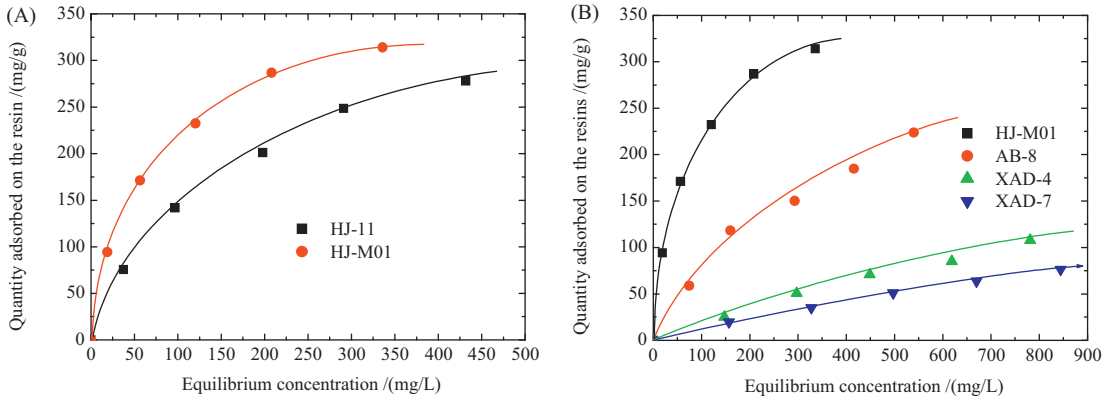

Fig. 5. Comparison of adsorption isotherms of salicylic acid on HJ-M01 with HJ-11 (A); and commercial resin AB-8, XAD-4 and XAD-7 (B) at 294 K.

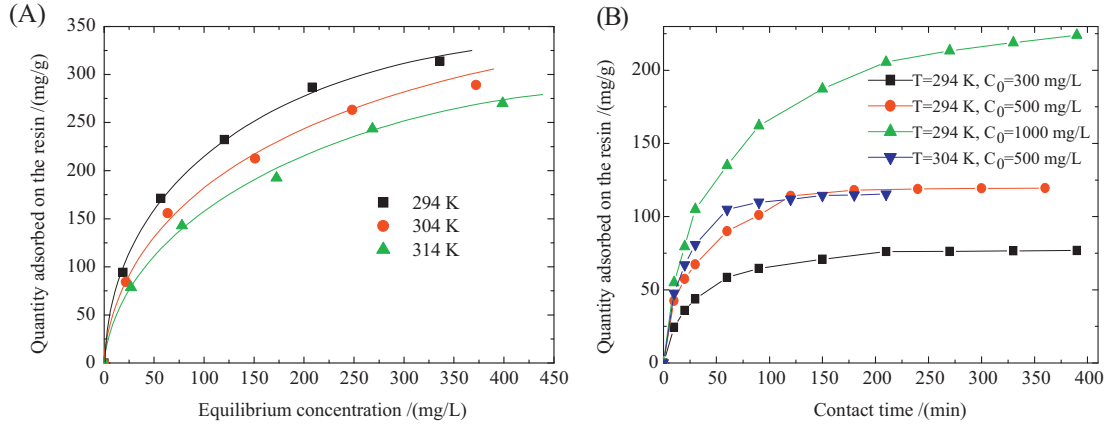

Fig. 7. Adsorption isotherms of salicylic acid on adsorbent HJ-M01 at 294, 304, and 314 K (A); and adsorption uptake curves for salicylic acid on adsorbent HJ-M01 at 294 and 304 K (B).

favorable for the adsorption while the anionic state of salicylic acid is unfavorable for the adsorption, especially the di-anion of salicylic acid cannot be adsorbed on HJ-M01. In particular, it is interesting to seen that the adsorption capacity of salicylic acid on HJ-M01 is also reduced as the solution pH decreases from 2.80 to 1.44. As the solution pH is lower than 2.80, the ionization equilibrium of salicylic acid will be affected due to the superfluous protons in aqueous solution and more salicylic acid molecules will be obtained, which should bring a few larger adsorption capacity on HJ-M01. Obviously, the deduction is opposite to the observation in Fig. 6. Note that there is 1.307 mmol/g of diethylenetriamine uploaded on the surface of HJ-M01 and these amino groups of diethylenetriamine should have an effect on the adsorption. The pK_{a1} of diethylenetriamine is determined to be 4.42 [49] and hence the dissociation curve of diethylenetriamine in aqueous solution is also predicted as a function of the solution pH. As the solution pH is lower than 2.80, more salicylic acid molecules are obtained while amino groups of diethylenetriamine uploaded on the surface of HJ-M01 are gradually protonized, which is disadvantageous for the adsorption. Hence the adsorption of salicylic acid is also reduced as the solution pH is lower than 2.80.

3.5. Adsorption equilibrium and adsorption thermodynamic parameters

The adsorption isotherms of salicylic acid on the resin HJ-M01 from aqueous solution at 294, 304 and 314 K are plotted in Fig. 7(A). An equilibrium capacity of 314.0 mg/g was obtained at a concentration of 335.9 mg/L and 294 K, suggesting that the resin HJ-M01 is a very efficient polymeric adsorbent for removing salicylic acid from aqueous solution. In addition, the adsorption capacity decreases with increasing temperature, implying that the adsorption is an exothermic process [25,47]. Table 2 lists the corresponding parameters for the Langmuir and Freundlich models. It is found that all of the adsorption isotherm data can be well fitted by Langmuir model ($R^2 > 0.99$).

The heat of adsorption, ΔH (kJ/mo1), adsorption free energy, ΔG (kJ/mo1) and adsorption entropy, ΔS (J/(mo1 K)) for the present adsorption system can be calculated as [50,51]:

$$\ln\ K_L = -\frac{\Delta H}{RT} + \ln K_0 \tag{5}$$

$$\Delta G = -RT\ \ln K_L \tag{6}$$

$$\Delta S = \frac{\Delta H - \Delta G}{T} \tag{7}$$

where R is the universal gas constant, 8.314 J/(mol K), T is the absolute temperature and K_0 is a constant. By plotting $\ln K_L$ versus $1/T$ (see Fig. S1), a straight line was obtained and ΔH was determined to be −18.38 kJ/mol. In addition, the positive ΔG indicates that the adsorption is an unfavorable process (see Table S3) and the negative ΔS suggests the adsorption system is more ordered after the adsorption.

3.6. Adsorption kinetics

Fig. 7(B) displays the adsorption kinetic curves of salicylic acid on resin HJ-M01 with initial concentrations at two 294 and 304 K. The adsorption kinetic data can be analyzed using different kinetic models. One of most widely used kinetic models is the Lagergren's rate equation [52]. The pseudo-first-order rate equation is given by:

$$\ln(q_e - q_t) = \ln\ q_e - k_1 t \tag{8}$$

where q_t and q_e are the adsorption amount at a given time t (s) and adsorption equilibrium, k_1 is the pseudo-first-order rate constant (min^{-1}).

The pseudo-second-order equation proposed by Ho and McKay [53,54] was also used to analyze the kinetic data:

$$\frac{t}{q_t} = \frac{1}{k_2 q_e^2} + \frac{1}{q_e} \tag{9}$$

where k_2 is the pseudo-second-order rate constant (g/(mg min)).

Both equations were used to correlate the adsorption kinetic data through linear regressions. Table 3 summarizes the corresponding model parameters. The much higher R^2 by the pseudo-second-order rate equation suggests that the adsorption kinetic data fitted by the pseudo-second-order rate equation is better.

In addition, we also applied a micropore diffusion model to analyze the adsorption kinetic data and to estimate the diffusion time constant. According to Ruthven et al. [55] for the fractional adsorption uptake (q_t/q_e) less than 85%, the adsorption kinetics in microporous adsorbents can be described by the following equation.

$$\frac{q_t}{q_e} = \frac{6}{\sqrt{\pi}}\sqrt{\frac{D_c t}{r_c^2} - \frac{3D_c t}{r_c^2}} \tag{10}$$

where D_c is the micropore diffusivity (cm^2/s) and r_c is the crystal diameter of the adsorbent (cm). The adsorption kinetic data shown in Fig. S2 were fitted to this micropore diffusion model through a nonlinear regression. The diffusion time constants (D_c/r_c^2) obtained

Table 2
Correlated parameters of the equilibrium data for the adsorption of salicylic acid on HJ-M01 from aqueous solution according to Langmuir and Freundlich equations.

T (K)	Langmuir equation				Freundlich equation				
	K_L (L/mg)	q_m (mg/g)		R^2	K_F ([(mg/g)(L/mg)$^{1/n}$])		n		R^2
		Values	Errors		Values	Errors	Values	Errors	
294	0.01579	371.7	$\pm 7.557 \times 10^{-5}$	0.9976	28.84	±0.07148	2.355	±0.03506	0.9799
304	0.01291	344.8	$\pm 1.198 \times 10^{-4}$	0.9948	23.50	±0.06792	2.301	±0.03228	0.9837
314	0.00977	333.3	$\pm 1.722 \times 10^{-5}$	0.9902	18.03	±0.05659	2.173	±0.02622	0.9902

Table 3
Constants of the kinetic data for the adsorption of salicylic acid on HJ-M01 from aqueous solution according to the first-order-rate and the pseudo-second-order rate equation.

	Pseudo-first-order rate equation					Pseudo-second-order rate equation			
	q_e (mg/g)		k_1 (min^{-1})		R^2	q_e (mg/g)		k_2 (g/(mg min))	R^2
	Values	Errors	Values	Errors		Values	Errors		
T = 294 K, C_0 = 300 mg/L	63.31	±0.1344	0.01852	$\pm 8.309 \times 10^{-4}$	0.9841	82.44	$\pm 1.213 \times 10^{-2}$	4.984×10^{-4}	0.9998
T = 294 K, C_0 = 500 mg/L	105.2	±0.08843	0.02269	$\pm 6.319 \times 10^{-4}$	0.9940	128.7	$\pm 7.770 \times 10^{-3}$	3.456×10^{-4}	0.9994
T = 294 K, C_0 = 1000 mg/L	182.5	±0.04490	0.01081	$\pm 2.776 \times 10^{-4}$	0.9948	247.5	$\pm 4.040 \times 10^{-3}$	9.350×10^{-5}	0.9995
T = 304 K, C_0 = 500 mg/L	86.57	±0.1304	0.02896	$\pm 1.360 \times 10^{-3}$	0.9847	124.8	$\pm 8.010 \times 10^{-3}$	5.395×10^{-4}	0.9996

from the non-linear regression were listed in Table S4. The diffusion activation energy E_a of 21.6 kJ/mol was estimated from the Arrhenius equation (Eq. (9)) using the diffusion time constants (C_0 = 500 mg/L) at 294 and 304 K.

$$\frac{D_c}{r_c^2} = K_A \exp\left(-\frac{E_a}{RT}\right) \tag{11}$$

3.7. Adsorption and desorption column dynamics

Adsorption column performance is a direct measure of an adsorbent's efficacy for wastewater treatment under application conditions. As can be seen in Fig. 8, the breakthrough point (C_v/C_0 = 0.05) of salicylic acid was measured to be 97.2 BV at an initial feed concentration of 1000.0 mg/L and its total adsorption throughput volume is 189.0 BV, confirming that the resin HJ-M01 is an efficient polymeric adsorbent for adsorptive removal of salicylic acid. The dynamic adsorption capacity of resin HJ-M01 was calculated using a numerical integration of the adsorption breakthrough curves by the following equation:

$$q_{\text{dynamic}}\ (\text{mg/g}) = \left\{\int_0^{\text{BV}_{\max}} \left(1 - \frac{C_V}{C_0}\right) \text{dBV}\right\} \times C_0(\text{mg/L}) \times \frac{10\ (\text{ml})}{3\ (\text{g})} \times \frac{1\ (\text{L})}{1000\ (\text{mL})} \tag{12}$$

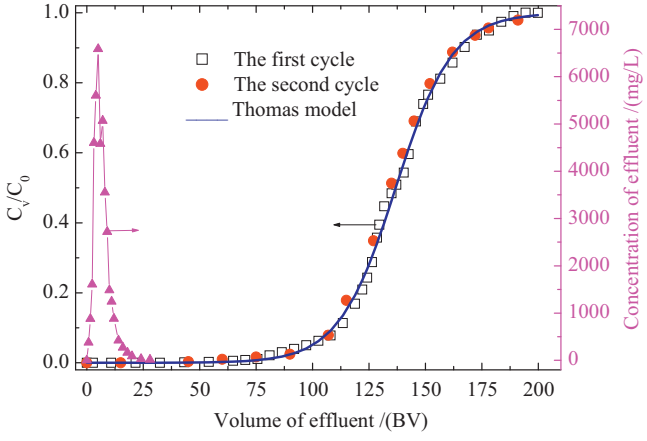

Fig. 8. Adsorption and desorption dynamic curves of salicylic acid from an adsorbent column packed with HJ-M01 at 294 K.

The dynamic adsorption capacity of salicylic acid on HJ-M01 estimated to be 456.4 mg/L at a feed concentration of 1000 mg/L and 294 K, which is between the extrapolated values from the Langmuir (349.6 mg/L) and the Freundlich models (541.9 mg/g).

We applied the Thomas model [56] to correlate the adsorption breakthrough curve. The Thomas model is given by:

$$\ln\left(\frac{C_0}{C_V} - 1\right) = \frac{k_T q_0 m}{Q} - \frac{k_T C_0 V_{\text{eff}}}{Q} \tag{13}$$

where k_T is the Thomas rate constant [ml/(h mg)], q_0 is the maximum solid-phase concentration of the adsorbate molecules (mg/g), m is the mass of adsorbent in the column (g), V_{eff} is the throughput volume (ml), and Q is the volumetric flow rate (60 ml/h). The adsorption breakthrough curve (C_v/C_0 vs. V_{eff}) were fitted to Thomas model using a non-linear regression. It is seen that the Thomas model fits the adsorption breakthrough curve very well. The model parameters obtained from the regression are: k_T = 0.4766 [ml/(h mg)] and q_0 = 45.6 mg/g, which are quite different from the 2nd order kinetic rate constant ($k_2 \cong 0.03$ ml/(h mg)) obtained from the adsorption kinetic data and the Langmuir monolayer adsorption capacity (q_m = 350 mg/g) calculated from the equilibrium data. This is probably because the feed concentration (1000 mg/L) used in the breakthrough test is much higher than those (<400 mg/L) used in the equilibrium and kinetic experiments.

After the first adsorption breakthrough experimental run the resin column was purged with deionized water and most of the adsorbed salicylic acid was effectively desorbed. The residual salicylic acid in the resin column was then desorbed with a 1% of sodium hydroxide aqueous solution. Only 25.0 bed volumes of 1% of sodium hydroxide solution were needed to completely regenerate the resin column. We estimated the desorption amount by the 1% of sodium hydroxide solution through a numerical integration of the desorption purge curve (effluent concentration vs. bed volume). It was found out that the desorption amount by 1% of sodium hydroxide solution is about 29.0% of the full adsorption capacity of the column, which suggests that 70% of the adsorbed salicylic acid in the resin column could be easily regenerated by purging with water. We also did the 2nd adsorption breakthrough run after the regeneration. It was shown that the 2nd breakthrough run is almost identical as the first one. This is a direct proof that the adsorption capacity of the resin column was fully recovered after regeneration with 1% of sodium hydroxide solution.

4. Conclusion

We have demonstrated the feasibility of tailoring pore textural property and surface functionality of polymeric adsorbents for selective adsorption of β-naphthol, phenol and salicylic acid from aqueous solution. Four hyper-cross-linked resins, HJ-11, HJ-33, HJ-55 and HJ-99 were synthesized by controlling the reaction time of self Friedel–Crafts reaction, then modified by the amination reaction with diethylenetriamine to produce the four resin samples HJ-M01, HJ-M03, HJ-M05 and HJ-M09. The samples synthesized in this work were characterized with N_2 adsorption–desorption, FT-IR, EDS, analysis of residual chlorine content and weak basic exchange capacity. The adsorption equilibrium, kinetics and column dynamics on resin HJ-M01 were performed to evaluate the efficacy of this promising adsorbent.

The experimental results indicated that longer Friedel–Crafts reaction times led to lower residual chlorine content, higher BET surface area and pore volume, and lower amino groups uploading after further amination reactions. It was possible to improve the adsorption capability and selectivity of the resins towards β-naphthol, phenol and salicylic acid from aqueous solution by adjusting the pore textural property (i.e. BET surface area, pore volume) and surface polarity. The sample HJ-M01 has shown significantly higher adsorption capacity for salicylic acid than its precursor HJ-01 and many commercial resins.

The Langmuir and Freundlich models correlate well the adsorption isotherms of salicylic acid on the resins, the pseudo-second-order rate and the micropore diffusion models describe well the adsorption kinetic data, and the Thomas model fits the adsorption breakthrough curve well. The dynamic adsorption capacity of salicylic acid on resin HJ-M01 was found to be 456.4 mg/L at a feed concentration of 1000 mg/L and 294 K, which matches well with the equilibrium adsorption capacity predicted by the Langmuir and the Freundlich models. The HJ-M01 column loaded with salicylic acid could be fully regenerated by purging with de-ionized water followed with 1% NaOH solution. A second adsorption breakthrough run on the regenerated resin HJ-M01 column was found to be similar as that of the first run. The polymeric adsorbents being developed have a great potential to replace commercial polymeric or activated carbon adsorbents for organic compounds removal from wastewater treatment.

Acknowledgment

The National Natural Science Foundation of China (No. 21174163), the Shenghua Yuying Project of Central South University, the Natural Science Foundation of Hunan Province (11JJ5007) and the Science and Technology Project of Hunan Province (2011SK3256) are gratefully acknowledged.

Appendix A. Supplementary data

Supplementary data associated with this article can be found, in the online version, at doi:10.1016/j.jhazmat.2012.03.053.

References

[1] S.J.T. Pollard, G.D. Fowlerr, C.J. Sollars, R. Perry, Low-cost adsorbents for waste and wastewater treatment: a review, Sci. Total Environ. 116 (1992) 31–52.
[2] J. Araña, E.P. Melián, V.M.R. López, A.P. Alonso, J.M.D. Rodríguez, O.G. Díaz, J.P. Peña, Photocatalytic degradation of phenol and phenolic compounds. Part I. Adsorption and FTIR study, J. Hazard. Mater. 146 (2007) 520–528.
[3] B. Pourabbas, B. Jamshidi, Preparation of MoS_2 nanoparticles by a modified hydrothermal method and the photo-catalytic activity of MoS_2/TiO_2 hybrids in photooxidation of phenol, Chem. Eng. J. 138 (2008) 55–62.
[4] S. Hamoudi, K. Belkacemi, F. Larachi, Catalytic oxidation of aqueous phenolic solutions catalyst deactivation and kinetics, Chem. Eng. Sci. 54 (1999) 3569–3576.
[5] A.G. Vlyssides, M. Loizidou, P.K. Karlis, A.A. Zorpas, D. Papaioannou, Electrochemical oxidation of a textile dye wastewater using a Pt/Ti electrode, J. Hazard. Mater. 70 (1999) 41–52.
[6] Z. Aksu, Application of biosorption for the removal of orange pollutants: a review, Process Biochem. 40 (2005) 997–1026.
[7] B.K. Körbahti, A. Tanyolaç, Continuous electrochemical treatment of phenolic wastewater in a tubular reactor, Water Res. 37 (2003) 1505–1514.
[8] H.T. Li, M.C. Xu, Z.Q. Shi, B.L. He, Isotherm analysis of phenol adsorption on polymeric adsorbents from nonaqueous solution, J. Colloid Interface Sci. 271 (2004) 47–54.
[9] K. László, P. Podkościelny, A. Dąbrowski, Heterogeneity of activated carbons with different surface chemistry in adsorption of phenol from aqueous solutions, Appl. Surf. Sci. 252 (2006) 5752–5762.
[10] S. Chakraborty, S. De, S. DasGupta, J.K. Basu, Adsorption study for the removal of a basic dye: experimental and modeling, Chemosphere 58 (2005) 1079–1086.
[11] J.H. Huang, Treatment of phenol and *p*-cresol in aqueous solution by adsorption using a carbonylated hypercrosslinked polymeric adsorbent, J. Hazard. Mater. 168 (2009) 1028–1034.
[12] J. Fan, W.B. Yang, A.M. Li, Adsorption of phenol, bisphenol A and nonylphenol ethoxylates onto hypercrosslinked and aminated adsorbents, React. Funct. Polym. 71 (2011) 994–1000.
[13] Z.Y. Xu, Q.X. Zhang, J.L. Chen, L.S. Wang, G.K. Anderson, Adsorption of naphthalene derivatives on hypercrosslinked polymeric adsorbents, Chemosphere 38 (1999) 2003–2011.
[14] M.P. Tsyurupa, V.A. Davankov, Porous structure of hypercrosslinked polystyrene: state-of-the-art mini-review, React. Funct. Polym. 66 (2006) 768–779.
[15] V. Davankov, M. Tsyurupa, Preparative frontal size-exclusion chromatography of mineral ions on neutral hypercrosslinked polystyrene, J. Chromatogr. A 1087 (2005) 3–12.
[16] V. Davankov, M. Tsyurupa, M. Ilyin, L. Pavlova, Hypercross-linked polystyrene and its potentials for liquid chromatography: a mini-review, J. Chromatogr. A 965 (2002) 65–73.
[17] A.M. Li, Q.X. Zhang, G.C. Zhang, J.L. Chen, Z.H. Fei, F.Q. Liu, Adsorption of phenolic compounds from aqueous solutions by a water-compatible hypercrosslinked polymeric adsorbent, Chemosphere 47 (2002) 981–989.
[18] V.A. Davankov, M.P. Tsyurupa, Structure and properties of hypercrosslinked polystyrene—the first representative of a new class of polymer networks, React. Polym. 13 (1990) 27–42.
[19] M.P. Tsyurupa, V.A. Davankov, Hypercrosslinked polymers: basic principle of preparing the new class of polymeric materials, React. Funct. Polym. 53 (2002) 193–203.
[20] X.H. Yuan, X.H. Li, E.B. Zhu, J. Hu, W.C. Sheng, S.S. Cao, A novel hypercrosslinked polymeric adsorbent modified by phenolic hydroxyl group of 2-naphthol with bromoethane as crosslinking reagent, Carbohydr. Polym. 74 (2008) 468–473.
[21] C.L. He, J.H. Huang, C. Yan, J.B. Liu, L.B. Deng, K.L. Huang, Adsorption behaviors of a novel carbonyl and hydroxyl groups modified hyper-cross-linked poly(styrene-co-divinylbenzene) resin for β-naphthol from aqueous solution, J. Hazard. Mater. 180 (2010) 634–639.
[22] C.G. Oh, J.H. Ahn, S.K. Ihm, Adsorptive removal of phenolic compounds by using hypercrosslinked polystyrenic beads with bimodal pore size distribution, React. Funct. Polym. 57 (2003) 103–111.
[23] J.H. Ahn, J.E. Jang, C.G. Oh, S.K. Ihm, J. Cortez, D.C. Sherrington, Rapid generation and control of microporosity, bimodal pore size distribution, and surface area in Davankov-type hyper-cross-linked resins, Macromolecules 39 (2006) 627–632.
[24] C.P. Wu, C.H. Zhou, F.X. Li, Experiments of Polymeric Chemistry, Anhui Science and Technology Press, Hefei, 1987.
[25] B.L. He, W.Q. Huang, Ion Exchange and Adsorption Resin, Shanghai Science and Technology Education Press, Shanghai, 1995.
[26] J.T. Wang, Q.M. Hu, B.S. Zhang, Y.M. Wang, Organic Chemistry, Nankai University Press, Tianjing, 1998.
[27] M.C. Xu, Z.Q. Shi, B.L. He, Structure and adsorption properties of hypercrosslinked polystyrene adsorbents, Acta Polym. Sin. 4 (1996) 446–449.
[28] G.H. Meng, A.M. Li, W.B. Yang, F.Q. Liu, X. Yang, Q.X. Zhang, Mechanism of oxidative reaction in the postcrosslinking of hypercrosslinked polymers, Eur. Polym. J. 43 (2007) 2732–2737.
[29] D.M. Ruthven, Principles and Adsorption and Adsorption Processes, Willey Inter-science, New York, 1984.
[30] J.H. Huang, K.L. Huang, S.Q. Liu, A.T. Wang, C. Yan, Adsorption of Rhodamine B and methyl orange on a hypercrosslinked polymeric adsorbent in aqueous solution, Colloids Surf. A 330 (2008) 55–61.
[31] E.V. Anslyn, D.A. Dougherty, Modern Physical Organic Chemistry, University Science, 2005.
[32] Q.W. Wang, Y.C. Yang, H.B. Gao, Problems on Hydrogen Bonding in Organic Chemistry, Tianjin University Press, Tianjin, 1993.
[33] M. Otero, C.A. Grande, A.E Rodrigues, Adsorption of salicylic acid onto polymeric adsorbents and activated charcoal, React. Funct. Polym. 60 (2004) 203–213.
[34] F.P. Bonina, M.L. Giannossi, L. Medici, C. Puglia, V. Summa, F. Tateo, Adsorption of salicylic acid on bentonite and kaolin and release experiments, Appl. Clay Sci. 36 (2007) 77–85.
[35] D. Kovačević, N. Kallay, I. Antol, A. Pohlmeier, H. Lewandowski, H.D Narres, The use of electrokinetic potential in the interpretation of adsorption phenomena: adsorption of salicylic acid on hematite, Colloids Surf. A 140 (1998) 261–267.
[36] J.E. Thomas, M.J. Kelley, The adsorption of salicylic acid onto γ-alumina and kaolinite from solution in hexane studied using diffuse reflectance infrared

Fourier transform spectroscopy (DRIFT), J. Colloid Interface Sci. 338 (2009) 389–394.
[37] M. Ukrainczyk, M. Gredičak, I. Jerić, D. Kralj, Interactions of salicylic acid derivatives with calcite crystals, J. Colloid Interface Sci. 365 (2012) 296–307.
[38] J.H. Huang, Hydroquinone modified hyper-cross-linked resin to be used as a polymeric adsorbent for adsorption of salicylic acid from aqueous solution, J. Appl. Polym. Sci. 121 (2011) 3717–3723.
[39] J.H. Huang, G. Wang, K.L. Huang, Enhanced adsorption of salicylic acid onto a β-naphthol-modified hyper-cross-linked poly(styrene-co-divinylbenzene) resin from aqueous solution, Chem. Eng. J. 168 (2011) 715–721.
[40] M. Otero, M. Zabkova, A.E. Rodrigues, Comparative study of the adsorption of phenol and salicylic acid from aqueous solution onto nonionic polymeric resins, Sep. Purif. Technol. 45 (2005) 86–95.
[41] B.J. Pan, B.C. Pan, W.M. Zhang, L. Lv, Q.X. Zhang, S.R. Zheng, Development of polymeric and polymer-based hybrid adsorbents for pollutants removal from waters, Chem. Eng. J. 151 (2009) 19–29.
[42] P.A.M. Freitas, K. Iha, M.C.F.C. Felinto, M.E.V Suárez-Iha, Adsorption of di-2-pyridyl ketone salicyloylhydrazone on Amberlite XAD-2 and XAD-7 resins: characteristics and isotherms, J. Colloid Interface Sci. 323 (2008) 1–5.
[43] M.S. Bilgili, Adsorption of 4-chlorophenol from aqueous solutions by xad-4 resin: isotherm, kinetic, and thermodynamic analysis, J. Hazard. Mater. 137 (2006) 157–164.
[44] J.R. Domínguez, T. González, P. Palo, E.M. Cuerda-Correa, Removal of common pharmaceuticals present in surface waters by Amberlite XAD-7 acrylic-ester-resin: Influence of pH and presence of other drugs, Desalination 269 (2011) 231–238.
[45] I. Langmuir, The constitution and fundamental properties of solids and liquids. Part I. Solids, J. Am. Chem. Soc. 38 (1916) 2221–2295.
[46] H.M.F. Freundlich, Über die adsorption in lösungen, Z. Phys. Chem. 57A (1906) 385–470.
[47] D.D. Duong, Adsorption Analysis: Equilibria and Kinetics, World Scientific Publishing, Singapore, 1998.
[48] S.O. Shan, D. Herschlag, Energetic effects of multiple hydrogen bonds, implications for enzymatic catalysis, J. Am. Chem. Soc. 118 (1996) 5515–5518.
[49] Y.H. Qiu, A.J. Huang, Y.L. Sun, Triethylamine or diethylenetriamine as dynamic modifier for suppressing basic protein adsorption in capillary electrophoresis, Chin. Chem. Lett. 10 (1999) 227–230.
[50] B.C. Pan, W.M. Zhang, B.J. Pan, H. Qiu, Q.R. Zhang, Q.X. Zhang, S.R. Zheng, Efficient removal of aromatic sulfonates from wasterwater by a recyclable polymer: 2-naphthalene sulfonate as a representative pollutant, Environ. Sci. Technol. 42 (2008) 7411–7416.
[51] İ. Uzun, F. Güzel, Rate studies on the adsorption of some dyestuffs and *p*-nitrophenol by chitosan and monocarboxymethylated (mcm)-chitosan from aqueous solution, J. Hazard. Mater. 118 (2005) 141–154.
[52] S. Lagergren, About the theory of so-called adsorption of soluble substances, Kungl. Svenska vetenskapsakademien. Handlingar. 24 (1898) 1–39.
[53] Y.S. Ho, Adsorption of heavy metals from waste streams by peat, PhD thesis, University of Birmingham, UK, 1995.
[54] Y.S. Ho, G.A. McKay, Comparison of chemisorption kinetic models applied to pollutant removals on various sorbents, Trans. I Chem. E 76 (1998) 332–338.
[55] D.M. Ruthven, S. Farooq, K.S. Knaebel, Pressure Swing Adsorption, VCH, New York, 1994.
[56] H.C. Thomas, Heterogeneous ion exchange in a flowing system, J. Am. Chem. Soc. 66 (1944) 1664–1666.